第38卷第1期
2022年1月

无 机 化 学 学 报
CHINESE JOURNAL OF INORGANIC CHEMISTRY

Vol.38 No.1
127-136

花状CeO_2/TiO_2异质结的构筑及光催化性能

王红侠*[,1,2] 李新星[1,2] 周 禹[1]

([1]宿迁学院信息工程学院,宿迁 223800)

([2]宿迁学院,宿迁市功能材料重点实验室,宿迁 223800)

摘要: 采用溶剂热法制备了三维花状CeO_2/TiO_2异质结光催化剂,然后以甲基橙(MO)为模拟有机污染物,在氙灯照射下考察了其光催化活性。结果表明,花状结构由纳米片和纳米颗粒复合而成,纳米片上均匀地附着CeO_2颗粒。Ce/Ti的物质的量之比(n_{Ce}/n_{Ti})和溶剂热时间影响异质结的光催化性能,当n_{Ce}/n_{Ti}=0.1、溶剂热时间为6 h时,CeO_2/TiO_2的光催化活性达到最佳,氙灯照射50 min的降解率达95%,光催化活性优于纯TiO_2,这主要是CeO_2和TiO_2形成了异质结,有利于光生电子和空穴的分离。

关键词: 异质结; 光催化; 光降解; 微纳结构; 半导体

中图分类号: O643; TQ134.1 **文献标识码:** A **文章编号:** 1001-4861(2022)01-0127-10

DOI: 10.11862/CJIC.2022.010

Constructing and Photocatalytic Performance of Flower-like CeO_2/TiO_2 Heterostructures

WANG Hong-Xia*[,1,2] LI Xin-Xing[1,2] ZHOU Yu[1]

([1]*Department of Information and Engineering, Suqian University, Suqian, Jiangsu* 223800, *China*)

([2]*Suqian Key Laboratory for Functional Materials, Suqian University, Suqian, Jiangsu* 223800, *China*)

Abstract: A kind of three-dimensional flower-like CeO_2/TiO_2 heterojunction as photocatalysts was designed by the solvothermal method. The photocatalytic activity was evaluated by the decomposition of methyl orange (MO) under xenon lamp irradiation. The results showed that the flower-like structure was composed of thin nanosheets, on which many CeO_2 particles were uniformly attached. The molar ratio of Ce to Ti (n_{Ce}/n_{Ti}) and the solvothermal time influenced on the photocatalytic performance. When n_{Ce}/n_{Ti}=0.1 and the solvothermal time was 6 h, the photocatalytic activity of CeO_2/TiO_2 reached the best, and the degradation rate reached 95% under xenon lamp irradiation for 50 min. The results suggested that the photocatalytic activity of CeO_2/TiO_2 heterojunction was greatly improved, compared to TiO_2, which was mainly the function of heterojunction formed by CeO_2 and TiO_2, and was conducive to the separation of photogenerated electrons and holes.

Keywords: heterostructure; photocatalysis; photodegradation; micro/nano-materials; semiconductor

0 Introduction

Photocatalytic technology can be used to simulate natural photosynthesis, which can change solar energy into chemical energy, and degrade organic pollutants in sewage into harmless substances such as CO_2 and H_2O under normal temperature and pressure[1-3], thus avoiding the secondary pollution problem with traditional methods. TiO_2 is an n-type semiconductor catalyst that is non-toxic, highly active, chemically stable,

收稿日期:2021-03-30。收修改稿日期:2021-10-29。

江苏省高等学校自然科学研究项目资助(No.19KJB430036)、江苏省高端结构材料重点实验室开放基金资助项目(No.hsm1907)、宿迁市科技计划项目(No.K202006)、宿迁学院新型复合材料研究创新团队(No.2021td01)和江苏省青蓝工程项目资助。

*通信联系人。E-mail:hongxia0816@163.com

cheap, environmentally friendly, and it has been widely studied as an ideal photocatalyst[4-7]. However, in the process of photocatalysis, TiO_2 has some defects, such as low quantum efficiency, easy recombination of electron-hole pairs, and low utilization of sunlight, which greatly restricts its extensive industrial application. The solution to these problems depends on in-depth and systematic basic research.

To improve the photocatalytic activity of TiO_2, the researchers used a variety of methods, such as controlling the morphology[8-11], doping transition metal ions and non-metallic ions[12-16], surface sensitization[17-18], semiconductor composite[19-20]. Recent studies show that the selection of semiconductors with appropriate energy bands to couple with TiO_2, such as Bi_2WO_6[21-22], g-C_3N_4[23-25], CdS[26-27], CeO_2[28-29], is conducive to separating electrons and holes, and improving the visible light catalysis of TiO_2. CeO_2 has high conductivity, thermal stability, oxygen storage capacity, and has a narrow energy gap (2.92 eV). Moreover, Ce^{4+} and Ce^{3+} ions are easy to reciprocal transformation, which makes CeO_2 have good electron transfer ability and light absorption ability. The bandgap difference between TiO_2 and CeO_2 can promote the separation of photogenerated electron-hole pairs and improve catalysis activity[30]. Although TiO_2 and CeO_2 composite materials have received extensive attention, the research of CeO_2/TiO_2 as promising photocatalytic materials is not deep enough. In particular, the photocatalytic efficiency of CeO_2/TiO_2 is far from practical application. Therefore, it is necessary to further improve the photocatalytic performance of CeO_2/TiO_2 by optimizing the experiment. In this work, we prepared CeO_2/TiO_2 photocatalyst materials with a three-dimensional flower structure by solvothermal method. Under xenon lamp irradiation, flower-like CeO_2/TiO_2 photocatalyst had high activity for methyl orange degradation.

1 Experimental

1.1 Preparation of the samples

Preparation of CeO_2: All the chemical reagents were chemically pure and were used directly without further processing. The water used was distilled water. Under strong stirring, 0.26 g cerium nitrate was dissolved in 100 mL water. After stirring frequently for 30 min, NaOH was added to the solution to control the pH to 9-10, followed by hydrothermal treatment at 180 ℃ in a Teflon-lined autoclave for 24 h. The product was centrifugally separated, washed with ethanol and distilled water, then dried. The sample was collected and then put into the annealing furnace at 500 ℃ for 2 h to obtain CeO_2.

Preparation of CeO_2/TiO_2: polyethylene glycol, cetyltrimethyl ammonium bromide, and carboxamide were immersed into 70 mL acetic acid solution, and after vigorous stirring to dissolve them, CeO_2 was added into the above-mixed solution, finally added 2 mL butyl titanate by dropping and stirring for 20 min, and then moved the solution to 100 mL stainless steel autoclave lined with polytetrafluoroethylene. The reaction time was different at 150 ℃, and cooling with the furnace to room temperature. The precipitates were washed with ethanol and water thoroughly three times, drying at 80 ℃ and calcining at 450 ℃ for 1 h. According to the above preparation method, the samples prepared with Ce/Ti molar ratios n_{Ce}/n_{Ti} of 0.05, 0.1 and 0.2 in the reaction system were marked as $0.05CeO_2/TiO_2$, $0.1CeO_2/TiO_2$, $0.2CeO_2/TiO_2$ respectively.

1.2 Characterization

Under the conditions of Cu target, 40 kV and 40 mA with Cu $K\alpha$ X-ray radiation source (λ=0.154 nm) and 2θ range of 20°-80°, the samples were recorded by X-ray diffractometer of Dandong Haoyuan instrument company; the morphologies of the synthetic samples were used by scanning electron microscope (SEM, Zeiss Merlin field emission) at the acceleration voltage of 5 kV; the specific surface area was measured using the measurement instrument (ASAP2460). The U-3900 ultraviolet-visible spectrophotometer with integrating sphere in Japan was used to measure the absorbance of powder. X-ray photoelectron spectroscopy (XPS) measurements were measured on an Escalab 250 Xi spectrometer. Photoluminescence (PL) spectra were measured using FLS 980 fluorescence spectrophotometer. The photocurrent response and electrochemical impedance spectroscopy (EIS) were carried by an electro-

chemical workstation (CHI660E).

1.3 Photocatalytic activity measurement

CeO_2/TiO_2 was added to methyl orange (MO) solution, then the MO solution was illuminated. The photocatalytic performance of the sample was tested by measuring the degradation rate of MO. The specific processes were listed as follows: 0.02 g of catalyst sample was added to 80 mL MO solution (10 mg·L^{-1}), and ultrasonic agitation was performed for 30 min to achieve adsorption-desorption equilibrium in the dark. A 300 W xenon lamp was used to simulate and irradiate from the top of the MO solution. The xenon lamp was 10 cm away from the liquid surface. A small portion of the solution was taken every 10 min to be centrifuged and separated. The absorbance of the residual MO was analyzed by an ultraviolet-visible spectrophotometer.

2 Results and discussion

2.1 Characterization of the samples

Fig. 1 shows the XRD patterns of CeO_2/TiO_2 heterojunction prepared by adding different amounts of CeO_2. There were several different diffraction peaks of CeO_2/TiO_2 heterojunction nanoflowers at 2θ =25.3°, 37.9°, 48.1°, 54.1°, 55.2°, 62.6°, and 70.3° respectively, corresponding to anatase TiO_2 (PDF No. 21-1272). The diffraction peaks with 2θ=28.6°, 33.2°, 56.6°, and 59.5° belong to the characteristic diffraction peaks of CeO_2 (PDF No. 34-0394), indicating that the heterostructure nanocomposite composed of TiO_2 and CeO_2. It can be seen from the figure that the intensity of the diffraction peak of CeO_2 increased gradually with the increase of CeO_2 content.

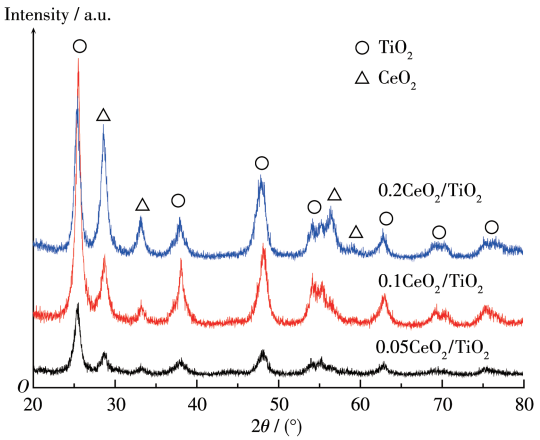

Fig.1　XRD patterns of CeO_2/TiO_2

Fig.2 showed that the prepared CeO_2/TiO_2 heterojunction had a three-dimensional flower-like structure, and nano-CeO_2 particles adhered to the petals of TiO_2. With the increase of CeO_2 content, the number of CeO_2 nanoparticles on the petals of TiO_2 increased gradually.

Solvothermal time can affect the morphology and properties of the samples. When the molar ratio of Ce and Ti was 0.1, and the samples were labeled as CeO_2/TiO_2-t, where t min was the reaction time. Fig.3 shows that the diffraction peaks correspond to the characteristic diffraction peaks of TiO_2 and CeO_2 respectively.

Fig.4 shows the SEM images of CeO_2/TiO_2. It can be seen that under solvothermal conditions for 4 h, the CeO_2/TiO_2 heterojunction was a three-dimensional flower-like microsphere structure. The diameter of the microspheres was between 0.61 and 0.96 μm. The average diameter was 0.77 μm. The flower structure was formed by the directional aggregation of nanoparticles. When the reaction time increased up to 6 h, the diameter of the flower-like microspheres ranged from 0.58 to 1.29 μm, with an average diameter of 0.59 μm. When the solvothermal time was 12 h, the diameter of the three-dimensional flower-like structure was 0.88-1.89 μm, with an average diameter of 1.36 μm. CeO_2 particles were oriented and integrated into a shuttle shape embedded between thin plates. With the increase of solvothermal time, the diameter of flower-like TiO_2 became smaller at the beginning and larger at the next stage, and CeO_2 gradually aggregated from nanoparticles to shuttle shape.

Fig. 5 shows the N_2 adsorption-desorption isotherms and BJH (Barrette-Joyner-Halenda) pore size distribution curves of samples. The Brunauer-Emmett-Teller specific surface area (S_{BET}), pore volume (V_P), and average pore size of the samples are shown in Table 1. The results showed the prepared samples had high S_{BET} and large V_P, providing more active sites and light-harvesting capacity, and improving the utilization efficiency of light, thereby contributing to the degradation of organic pollutants.

Fig.6 shows the full spectrum of CeO_2/TiO_2-6 and

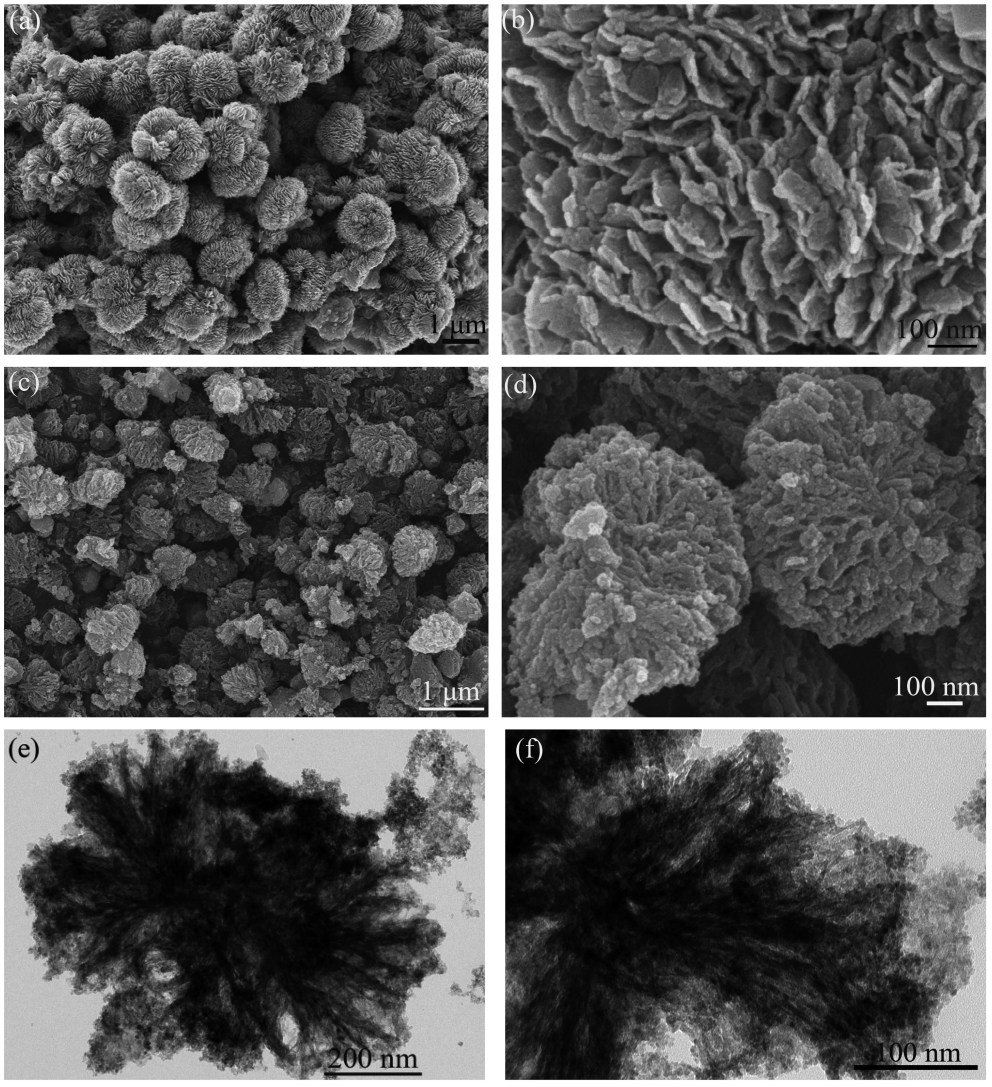

Fig.2 SEM and TEM images of (a, b) 0.05CeO_2/TiO_2, (c, d) 0.1CeO_2/TiO_2, and (e, f) 0.2CeO_2/TiO_2

the high-resolution XPS spectra of Ti2*p*, O1*s*, and Ce3*d*. It can be seen from Fig.6a that the sample only contained C, O, Ti, and Ce elements. C was mainly derived from the residual carbon of some organic precursors during heat treatment and the oily carbon from the XPS instrument itself. The binding energies of 458.78 and 464.48 eV in Fig.6b correspond to the characteristic peaks of Ti2$p_{2/3}$ and Ti2$p_{1/2}$ orbits respectively, which are the standard bond energies of Ti2*p* in pure TiO_2, indicating that Ti exists in form of Ti^{4+} [31]. In the O1*s* spectrum of Fig.6c, one peak at around 530.10 eV corresponds to the oxygen in the TiO_2 lattice, and the other peak at around 531.58 eV corresponds to the hydroxyl (—OH) on the surface of TiO_2 [32-33]. In Fig.6d, V (881.52), V″ (888.13), and V‴ (898.41) correspond to Ce3$d_{5/2}$ spin-orbital bands; U (900.11), U″ (906.83), and U‴ (915.81) correspond to Ce3$d_{3/2}$ spin - orbital bands. The peaks labeled as V, V″, V‴, U, U″, and U‴ are attributed to the existence of Ce^{4+}. The peaks at V′

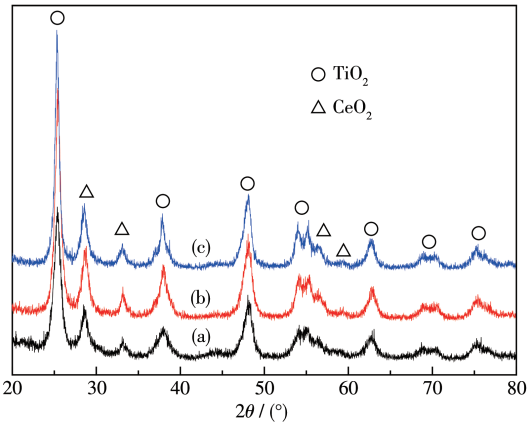

Fig.3 XRD patterns of (a) CeO_2/TiO_2-4, (b) CeO_2/TiO_2-6 and (c) CeO_2/TiO_2-12

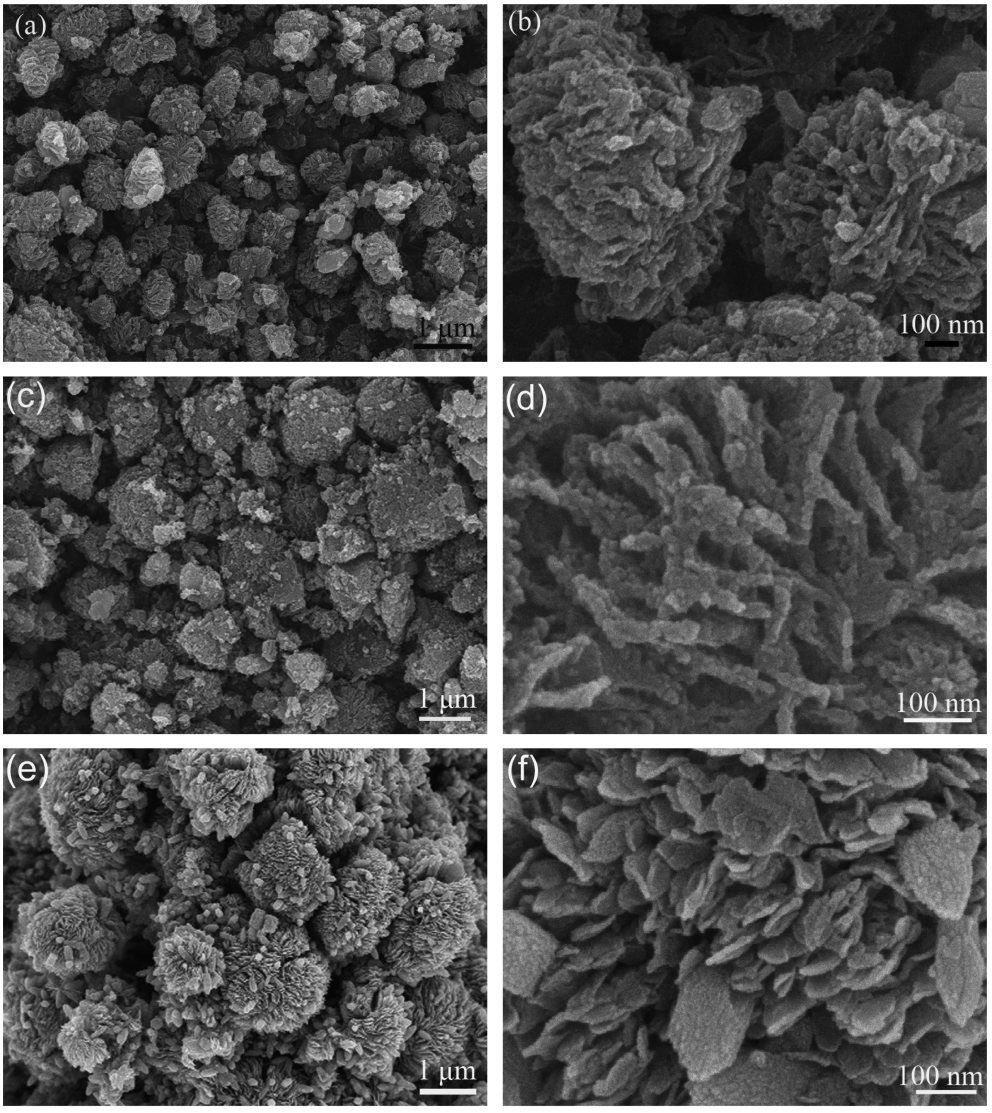

Fig.4　SEM images of (a, b) CeO_2/TiO_2-4, (c, d) CeO_2/TiO_2-6 and (e, f) CeO_2/TiO_2-12

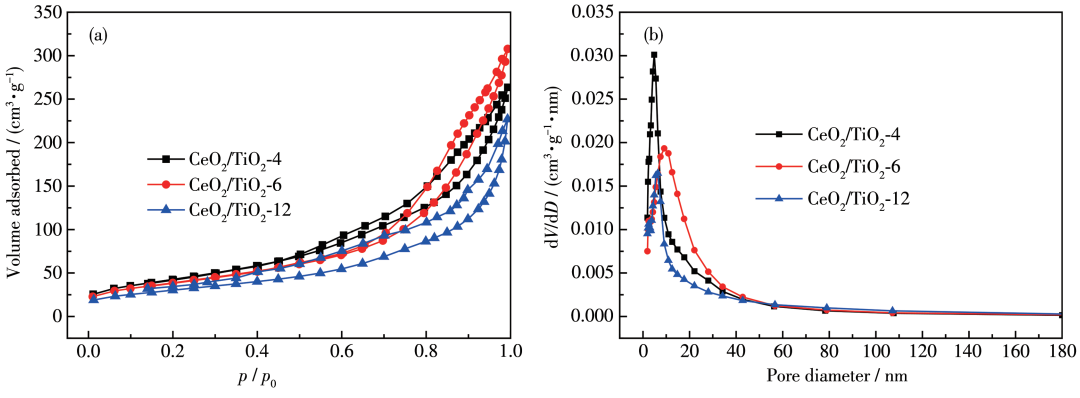

Fig.5　(a) N_2 adsorption-desorption isotherms and (b) pore size distribution curves for CeO_2/TiO_2-*t*

(885.13) and U′ (903.12) are attributed to the presence of Ce^{3+} in the composite[34]. Ce^{3+} is mainly due to the strong interaction between TiO_2 and CeO_2, which makes Ce^{4+} reduced to Ce^{3+}[35].

Because the intensity of light emission depends on the recombination ability of excited electrons and holes, we can analyze the ability of semiconductor materials to capture and migrate photogenerated holes

Table 1 S_{BET}, V_P, and average pore diameter of CeO_2/TiO_2-*t*

Sample	S_{BET} / ($m^2 \cdot g^{-1}$)	V_P / ($cm^3 \cdot g^{-1}$)	Average pore diameter / nm
CeO_2/TiO_2-4	159	0.41	8.68
CeO_2/TiO_2-6	143	0.48	11.44
CeO_2/TiO_2-12	110	0.36	11.48

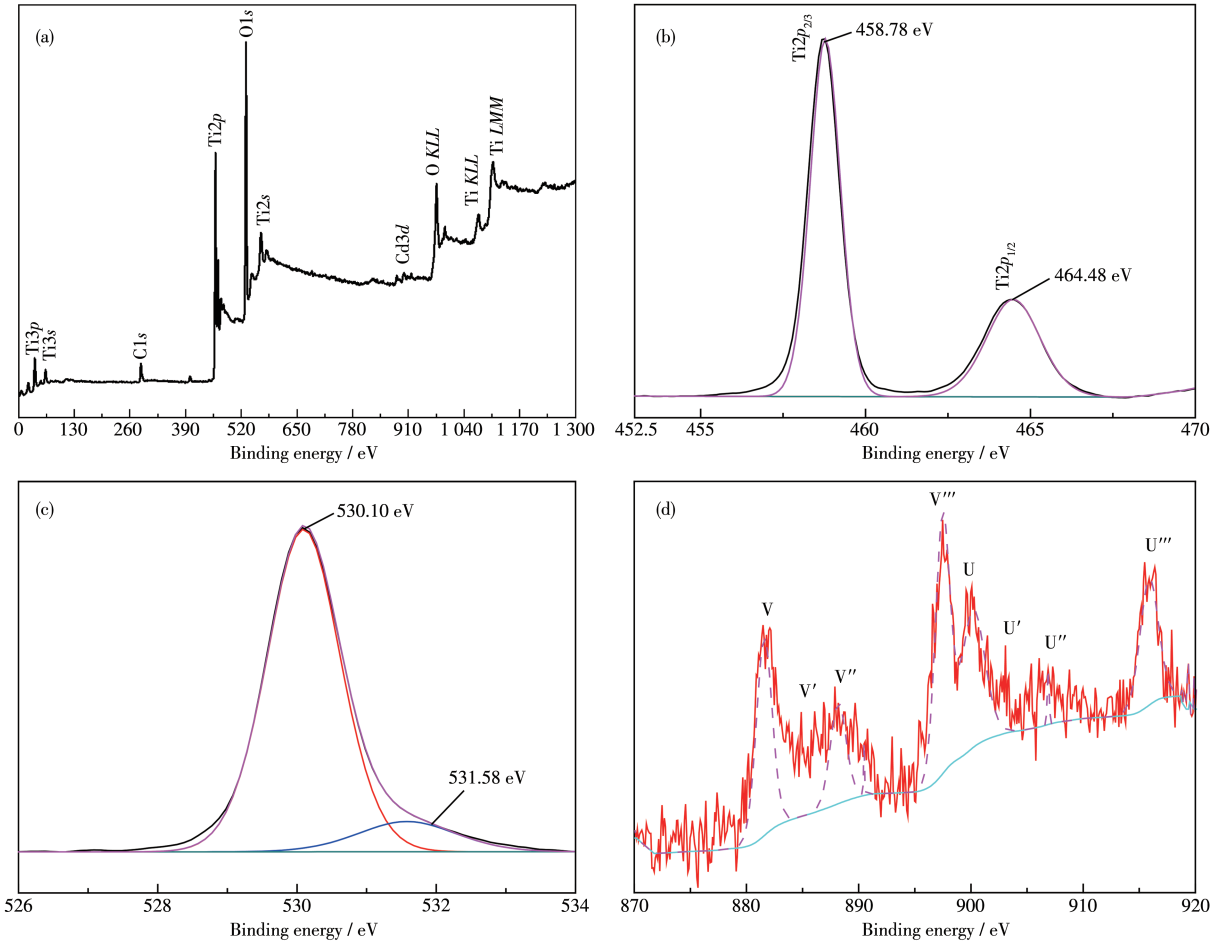

Fig.6 XPS spectra of CeO_2/TiO_2-6: (a) survey, (b) Ti2*p*, (c) O1*s*, (d) Ce3*d*

and electrons. The low intensity of the PL spectrum indicates that the recombination rate of electron-hole pairs is low and the separation efficiency of electron-hole pairs represents reverse. Fig.7 shows the PL spectra excited at 350 nm. The PL intensity of CeO_2/TiO_2-12 was lower than that of CeO_2/TiO_2-6, indicating that CeO_2/TiO_2-12 presented high separation efficiency.

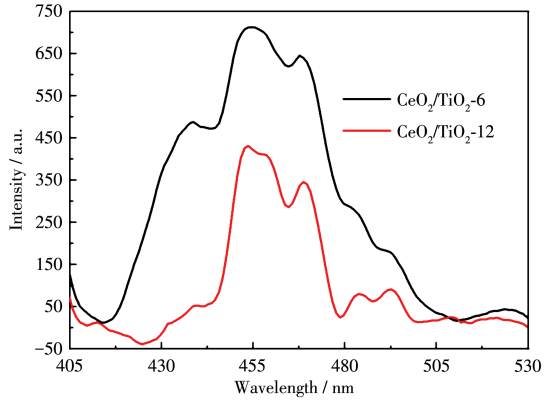

Fig.7 PL spectra of CeO_2/TiO_2-6 and CeO_2/TiO_2-12

2.2 Photocatalytic activity

To investigate the photocatalytic activity of the sample, the photocatalytic degradation of MO (xenon lamp simulated sunlight) was carried out. The degradation rate of MO was calculated as follows: $D=(1-A/A_0)\times 100\%$, where D is the degradation rate of MO solution; A_0 is the absorbance of MO solution before irradiation; A is the absorbance of MO solution at the wavelength of

464 nm. The experimental results of photocatalysis under light were shown in Fig.8.

Fig.8a shows the curve of the photocatalytic degradation rate of MO under simulated sunlight for the samples prepared with various molar ratios of CeO_2 and TiO_2. Fig.8b shows the photocatalytic degradation rate curves of MO under simulated sunlight irradiation for the samples prepared under different solvothermal times when the molar ratio of CeO_2 to TiO_2 was 0.1 (The material prepared without polyethylene glycol, cetyltrimethylammonium bromide, and carboxamide was recorded as CeO_2/TiO_2-B). It can be seen that the degradation rate of MO with catalyst increased with the extension of illumination time. The degradation rate of CeO_2/TiO_2 was better than that of TiO_2 after 50 min illumination. The photocatalytic performance of flower-like CeO_2/TiO_2 was higher than that of CeO_2/TiO_2-B. $0.1CeO_2/TiO_2$ had the best photocatalytic performance under 50 min illumination and the photocatalytic activity of CeO_2/TiO_2-6 was the best, and the degradation rate reached 95% after 50 min illumination (Fig. 8b).

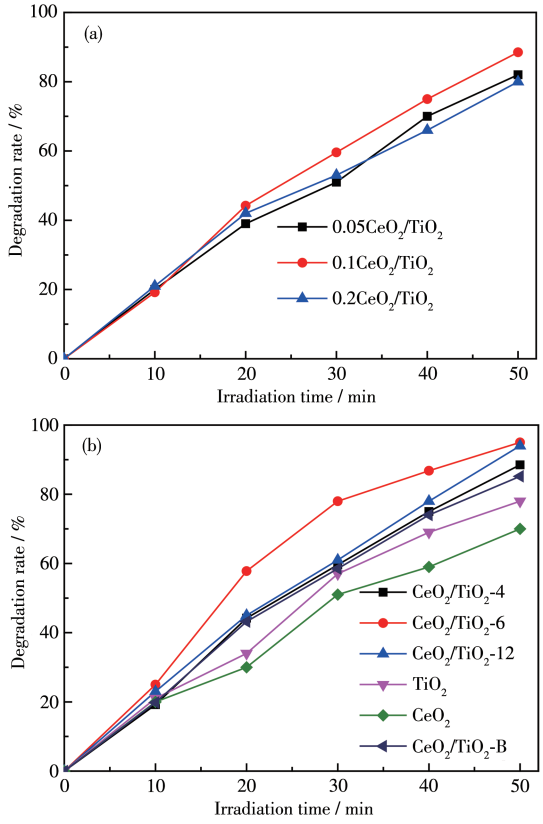

Fig.8　Photocatalytic degradation rate of MO for the samples

The degradation rate of MO solution added with pure TiO_2 or CeO_2 was only 78% or 70% respectively after 50 min illumination, which indicated that the composite of CeO_2 and TiO_2 enhances the photocatalytic activity of TiO_2.

Fig.9 is the UV-Vis diffuse reflectance spectra of the samples. It can be seen that the absorption band edges of TiO_2, CeO_2, CeO_2/TiO_2-4, CeO_2/TiO_2-6, and CeO_2/TiO_2-12 were 393, 432, 463, 481, and 469 nm respectively. According to the formula E_g=1 240/λ_g (λ_g is absorption edge), the bandgaps (E_g) of TiO_2, CeO_2, CeO_2/TiO_2-4, CeO_2/TiO_2-6, and CeO_2/TiO_2-12 were about 3.16, 2.87, 2.68, 2.58, and 2.64 eV respectively, which indicates that CeO_2/TiO_2 broadens the absorption range compared with TiO_2 and CeO_2.

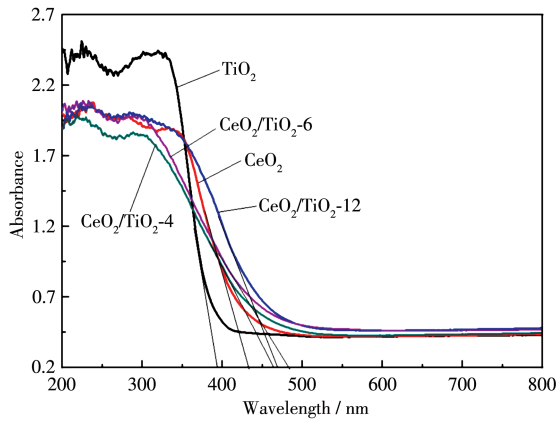

Fig.9　UV-Vis diffuse reflectance spectra of the samples

Fig.10 shows the effects of reuse times of CeO_2/TiO_2-6 catalyst on photocatalytic activity. It can be seen that the degradation rates of MO by CeO_2/TiO_2-6 were 95%, 94%, and 92% respectively when the cata-

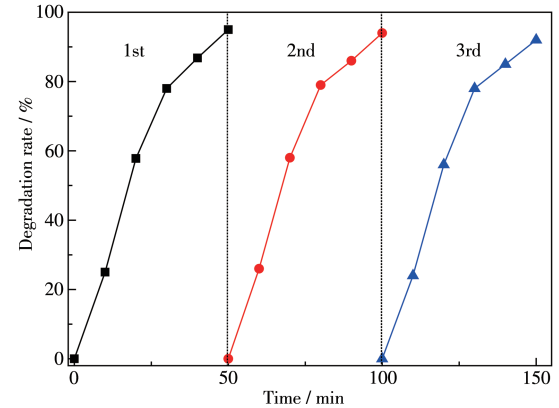

Fig.10　Effect of reuse degradation times of CeO_2/TiO_2-6 on the degradation rate of MO

lyst was reused for the first time, the second time, and the third time. The catalytic activity was not significantly reduced, indicating that the photocatalyst has certain stability and can be recycled many times.

In the process of photocatalysis, water molecules or hydroxyl radicals can be oxidized by holes to generate hydroxyl radicals, and superoxide anion radicals may be generated when dissolved oxygen in water receives photogenerated electrons. Electron spin resonance (ESR) is generally used to detect hydroxyl radical (·OH) radical and superoxide radical ($\cdot O_2^-$). Fig.11 presents the ESR spectra of DMPO-·OH and DMPO-$\cdot O_2^-$ obtained with 5,5-dimethyl-1-pyrroline *N*-oxide (DMPO) as the radical scavenger. Under xenon lamp irradiation, the ESR spectra of ·OH showed four characteristic peaks, and that of $\cdot O_2^-$ showed six characteristic peaks. However, there was no signal in the dark. It indicates that ·OH and $\cdot O_2^-$ exist in the reaction system with CeO_2/TiO_2.

The interface charge transfer and photogenerated charge recombination of the catalyst were investigated by electrochemical characterization. Fig.12a shows the photocurrent response of the catalyst under xenon lamp irradiation. It suggests that CeO_2, TiO_2, and CeO_2/TiO_2-6 all had obvious photocurrent responses. When the light source was turned off, the current signal returned to the original level, and the response current of CeO_2/TiO_2-6 was higher than that of pure CeO_2 or pure TiO_2 under the light. Generally, the stronger the separation ability of photo-generated carriers, the stronger the photocurrent of the material. That shows the separation ability of CeO_2/TiO_2-6 photo-generated carriers was better than pure CeO_2 and TiO_2, which is mainly due to the formation of heterojunction between CeO_2 and TiO_2. EIS can further confirm the effective separation of photogenerated electrons and holes. The arc radius in EIS (Fig.12b) is related to the charge transfer resistance of the material. In general, the smaller the arc radius, the faster the separation or transfer speed of photogenerated carriers, and the photocurrent intensity is also

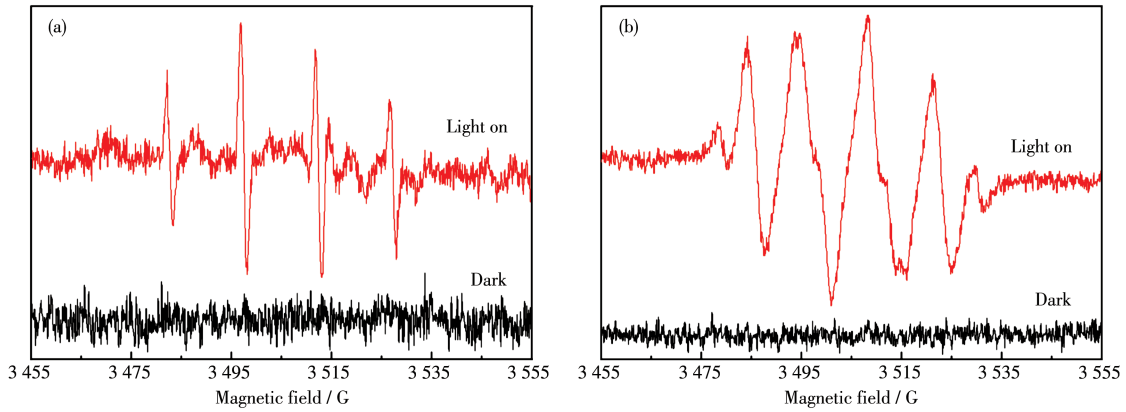

Fig.11 ESR spectra of (a) DMPO-·OH and (b) DMPO-$\cdot O_2^-$ for CeO_2/TiO_2-6 in the dark and under xenon lamp irradiation

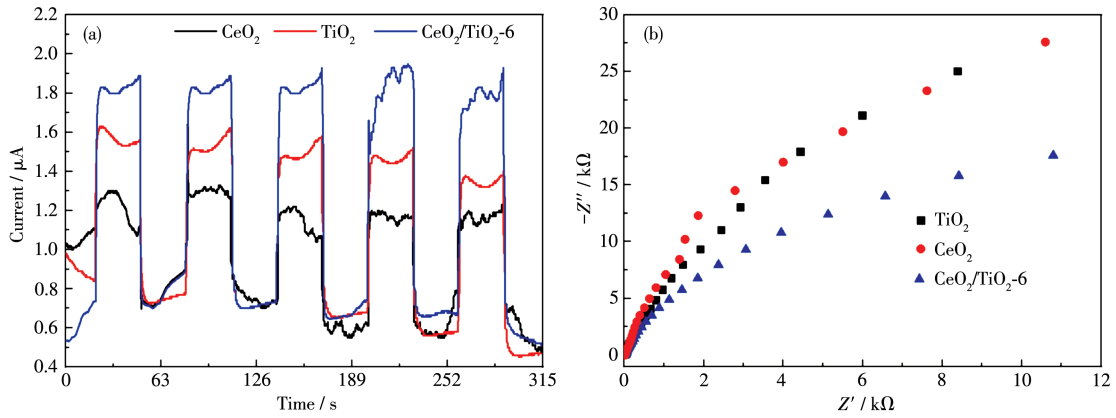

Fig.12 (a) Transient photocurrent responses of CeO_2, TiO_2, and CeO_2/TiO_2-6; (b) EIS spectra of CeO_2, TiO_2, and CeO_2/TiO_2-6

increased. It can be seen that CeO_2/TiO_2-6 had the smallest arc radius, which indicates that CeO_2/TiO_2-6 has the smallest electron transfer resistance and the best charge separation efficiency, which is consistent with the photocurrent response.

Fig. 13 shows the photocatalysis mechanism of CeO_2/TiO_2. Under simulated sunlight, CeO_2/TiO_2 can absorb not only ultraviolet light but also visible light. Both CeO_2 and TiO_2 can be excited by ultraviolet light, then the electrons jump to the conduction band to form the conduction band electron (e^-) while leaving holes (H^+) in the valence band. Because the conduction band (CB) of CeO_2 is higher than that of TiO_2, the electrons in CB of CeO_2 transfer to CB of TiO_2 through the interface. On the other hand, the valence gap (VB) of CeO_2 is lower than that of TiO_2, and the holes of VB of TiO_2 are transferred to VB of CeO_2, which is prone to the separation of photogenerated electron-hole pairs[30]. Under visible light irradiation, electrons from VB of CeO_2 are transferred to CB of TiO_2, and photogenerated electrons in CB of CeO_2 can be transferred to CB of TiO_2, thus inhibiting the recombination of photogenerated electrons and hole[36]. The results were consistent with the photocurrent response and EIS. Subsequently, the e^- was reacted with the O_2 to form $\cdot O_2^-$. The H_2O could be oxidized by h^+ to produce ·OH. The pollutant was oxidized by $\cdot O_2^-$ and ·OH to produce CO_2 and H_2O. Simultaneously, the h^+ in VB of CeO_2 was directly involved in the oxidation of pollutants.

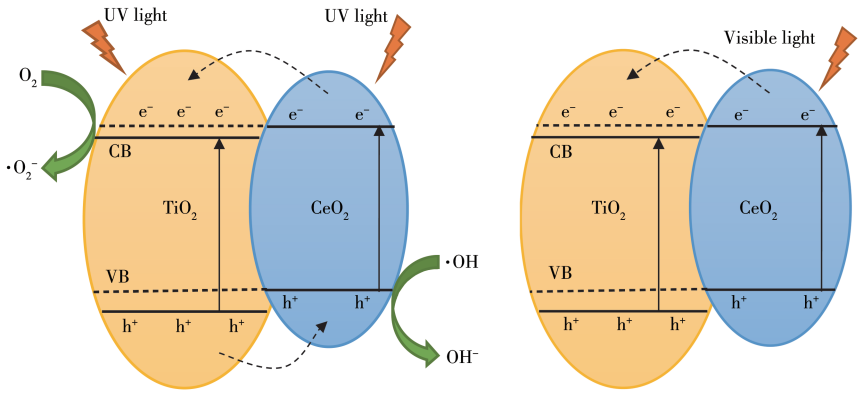

Fig.13　Photocatalysis mechanism of CeO_2/TiO_2

3　Conclusions

The three-dimensional flower-like CeO_2/TiO_2 heterojunction was prepared by the solvothermal method. Compared with TiO_2, flower-like CeO_2/TiO_2 heterojunction showed better photocatalytic performance under simulated sunlight. Among them, the degradation rate of MO reached 95% when CeO_2/TiO_2-6 was illuminated for 50 min, and the photocatalytic performance reached the best. The flower-like CeO_2/TiO_2 heterojunction had excellent catalytic performance, which is mainly due to the following factors. First of all, the three-dimensional hierarchical structure, with a large specific surface area and a different size of pore structure, greatly improves the utilization of light. Secondly, the heterojunction effect can enhance the efficiency of charge separation and interface charge transfer greatly.

References:

[1]Nakata K, Fujishima A. TiO_2 Photocatalysis: Design and Applications. *J. Photochem. Photobiol. C*, **2012**,**13**(3):169-189

[2]Xiong Z G, Dou H Q, Pan J H, Ma J Z, Xun C, Zhao X S. Synthesis of Mesoporous Anatase TiO_2 with a Combined Template Method and Photocatalysis. *CrystEngComm*, **2010**,**12**(11):3455-3457

[3]Schneider J, Matsuoka M, Takeuchi M, Zhang J L, Horiuchi Y, Anpo M, Bahenmann D W. Understanding TiO_2 Photocatalysis: Mechanisms and Materials. *Chem. Rev.*, **2014**,**114**(19):9919-9986

[4]Ma Y, Wang X L, Jia Y S, Chen X B, Han H X, Li C. Titanium Dioxide-Based Nanomaterials for Photocatalytic Fuel Generations. *Chem. Rev.*, **2014**,**114**(19):9987-10043

[5]Chen X B, Liu L L, Yu P Y, Mao Y. Increasing Solar Absorption for Photocatalysis with Black Hydrogenated Titanium Dioxide Nanocrystals. *Science*, **2011**,**331**:746-750

[6]Zhang J, Xu L J, Zhu Z Q, Liu J Q. Synthesis and Properties of (Yb, N)-TiO_2 Photocatalyst for Degradation of Methylene Blue (MB) under Visible Light Irradiation. *Mater. Res. Bull.*, **2015**,**70**:358-364

[7]Zou X X, Li G D, Wang K X, Lu L, Su J, Chen J S. Light-Induced Formation of Porous TiO_2 With Superior Electron - Storing Capacity. *Chem. Commun.*, **2010**,**46**:2112-2114

[8]Kim M H, Baik J M, Zhang J P, Larson C, Li Y L, Stucky G D, Moskovits M, Wodtke A M. TiO_2 Nanowire Growth Driven by Phosphorus-Doped Nanocatalysis. *J. Phys. Chem. C*, **2010**,**114**(24):10697-10702

[9]Souni M E, Habouti S, Pfeiffer N, Lahmar A, Dietze M, Solterbeck C H. Brookite Formation in TiO_2-Ag Nanocomosites and Visible-Light-Induced Templated Growth of Ag Nanostructures in TiO_2. *Adv. Funct. Mater.*, **2010**,**20**(3):377-385

[10]Ye J F, Liu W, Cai J G, Chen S, Zhao X W, Zhou H H, Qi L M. Nanoporous Anatase TiO_2 Mesocrystals: Additive-Free Synthesis, Remarkable Crystalline-Phase Stability, and Improved Lithium Insertion Behavior. *J. Am. Chem. Soc.*, **2011**,**133**(4):933-940

[11]Li G L, Chen Q W, Lan J. Facile Synthesis, Metastable Phase Induced Morphological Evolution and Crystal Ripening, and Structure-Dependent Photocatalytic Properties of 3D Hierarchical Anatase Superstructures. *ACS Appl. Mater. Interfaces*, **2014**, **6**(24): 22561 - 22568

[12]Pan X, Xu Y J. Defect Mediated Growth of Noble Metal (Ag, Pt and Pd) Nanoparticles on TiO_2 with Oxygen Vacancies for Photocatalytic Redox Reactions under Visible Light. *J. Phys. Chem. C*, **2013**, **117** (35):17996-18005

[13]Choi H J, Kang M. Hydrogen Production from Methanol/Water Decomposition in a Liquid Photosystem Using the Anatase Structure of Cu Loaded TiO_2. *Int. J. Hydrogen. Energy*, **2007**,**32**:3841-3848

[14]Zhang L, Li L, Mou Z G, Li X F. Study on Microstructure and Catalytic Performance of B, C, N Co-dopped TiO_2. *Procedia Eng.*, **2012**, **27**:552-556

[15]Yan J K, Gan G Y, Du J H, Yi J H. Formation Mechanism of Secondary Phase in (La, Nb) Codoped TiO_2 Ceramics Varistor. *Procedia Eng.*, **2012**,**27**:1271-1283

[16]Khaki M R D, Shafeeyan M S, Raman A A A, Daud W M A W. Evaluating the Efficiency of Nano-Sized Cu Doped TiO_2/ZnO Photocatalyst under Visible Light Irradiation. *J. Mol. Liq.*, **2018**,**258**:354-365

[17]Wang K T, Lu N, Chu C W, Feng T Y, Kung C C, Tu W H, Yeh Y P, Francisco J S. Robust Sensitizer-Assisted Platinized Titanium Dioxide in Photocatalytic Removal of 4 - Chlorophenol in Water: Light Tunable Sensitizer. *J. Photoch. Photobio. A*, **2018**,**358**:100-110

[18]Endo R, Siriwardena H D, Kondo A, Yamaoto C, Shimomura M. Structural and Chemical Analysis of TiO_2 Nanotube Surface for Dye-Sensitized Solar Cells. *Appl. Surf. Sci.*, **2018**,**439**:954-962

[19]杨冰叶, 李航, 商宁昭, 冯成, 高书涛, 王春. 中空花状可见光响应催化剂 g-C_3N_4@BiOCl 的制备及其光催化活性. 无机化学学报, **2017**,**33**(3):396-404
YANG B Y, LI H, SHANG N Z, FENG C, GAO S T, WANG C. Visible-Light Responsive Photocatalyst g-C_3N_4@BiOCl with Hollow Flower-like Structure: Preparation and Photocatalytic Performance. *Chinese J. Inorg. Chem.*, **2017**,**33**(3):396-404

[20]Rodrígueza D S, Medranob M G M, Barriosa H R V E. Photocatalytic Properties of BiOCl-TiO_2 Composites for Phenol Photodegradation. *J. Environ. Chem. Eng.*, **2018**,**6**:1601-1612

[21]Guo Q Y, Huang Y F, Xu H, Luo D, Huang F Y, Gu L, Wei Y L, Zhao H, Fan L Q, Wu J H. The Effects of Solvent on Photocatalytic Properties of Bi_2WO_6/TiO_2 Heterojunction under Visible Light Irradiation. *Solid State Sci.*, **2018**,**78**:95-106

[22]Du Z F, Cheng C, Tan L, Lan J W, Jiang S X, Zhao L D, Guo R H. Enhanced Photocatalytic Activity of Bi_2WO_6/TiO_2 Composite Coated Polyester Fabric under Visible Light Irradiation. *Appl. Surf. Sci.*, **2017**,**435**:626-634

[23]Wang X Q, Wang F, Chen B, Cheng K, Wang J L, Zhang J J, Song H. Promotion of Phenol Photodecomposition and the Corresponding Decomposition Mechanism over g-C_3N_4/TiO_2 Nanocomposites. *Appl. Surf. Sci.*, **2018**,**453**:320-329

[24]Zhong R Y, Zhang Z S, Yi H Q, Zeng L, Tang C, Huang L M, Gu M. Covalently Bonded 2D/2D O-g-C_3N_4/TiO_2 Heterojunction for Enhanced Visible - Light Photocatalytic Hydrogen Evolution. *Appl. Catal. B*, **2018**,**237**:1130-1138

[25]Li C Q, Sun Z M, Xue Y L, Yao G Y, Zheng S L. A Facile Synthesis of g - C_3N_4/TiO_2 Hybrid Photocatalysts by Sol - Gel Method and Its Enhanced Photodegradation Towards Methylene Blue under Visible Light. *Adv. Powder Technol.*, **2016**,**27**:330-337

[26]Su S, Ma J W, Zuo W L, Wang J, Liu L, Feng S, Liu T, Fu W Y, Yang H B. Nanoforest - like CdS/TiO_2 Heterostructure Composite: Synthesis and Photoelectrochemical Application. *Chin. Phys. B*, **2018**,**8**:680-685

[27]Yang X D, Wang Y Q, Wang Z S, Lv X Z, Jia H X, Kong J H, Yu M H. Preparation of CdS/TiO_2 Nanotube Arrays and the Enhanced Photocatalytic Property. *Ceram. Int.*, **2016**,**42**(6):7192-7202

[28]Zahoor M, Arshad A, Khan Y, Iqbal M, Bajwa S Z, Soomro R A, Ahmad I, Butt F K, Iqbal M Z, Wu A, Khan W S. Enhanced Photocatalytic Performance of CeO_2-TiO_2 Nanocomposite for Degradation of Crystal Violet Dye and Industrial Waste Effluent. *Appl. Nanosci.*, **2018**,**8**:1091-1099

[29]Wang J, Shi Z N, Zhou R X. High Activity of CeO_2-TiO_2 Composites for Deep Oxidation of 1,2-Dichlorethane. *J. Rare Earths*, **2020**,**8**:906-911

[30]Fan Z H, Meng F M, Gong J F, Li H J, Hu Y D, Liu D R. Enhanced Photocatalytic Activity of Hierarchical Flower-like CeO_2/TiO_2 Heterostructures. *Mater. Lett.*, **2016**,**175**:36-39

[31]Parveen N, Ansari M O, Han T H, Cho M H. Simple and Rapid Synthesis of Ternary Polyaniline/Titanium Oxide/Graphene by Simultaneous TiO_2 Generation and Aniline Oxidation as Hybrid Materials for Supercapacitor Applications. *J. Solid State Electrochem.*, **2017**, **21**:57-68

[32]Liu R, Li H, Duan L, Shen H, Zhang Y, Zhao X. *In-Situ* Synthesis and Enhanced Visible Light Photocatalytic Activity of C-TiO_2 Microspheres/Carbon Quantum Dots. *Ceram. Int.*, **2017**,**43**(12):8648-8654

[33]Fiorenza R, Bellardita M, Barakat T, Scirè S, Palmisano L. Visible Light Photocatalytic Activity of Macro-mesoporous TiO_2-CeO_2 Inverse Opals. *J. Photoch. Photobio. A*, **2018**,**352**:25-34

[34]Wang X Q, Xu H L, Luo X H, Li M, Dai M, Chen Q H, Song H. Enhanced Photocatalytic Properties of CeO_2/TiO_2 Heterostructures for Phenol Degradation. *Colloid Interface Sci. Commun.*, **2021**, **44**: 100476-100487

[35]Basha M H, Gopal O N. Solution Combustion Synthesis and Characterization of Phosphorus Doped TiO_2-CeO_2 Nanocomposite for Photocatalytic Applicationsopals. *Mat. Sci. Eng. B*, **2018**,**236**:43-47

[36]Tian J, Sang Y H, Zhao Z H, Zhou W J, Wang D Z, Kang X L, Liu H, Wang J Y, Chen S W, Cai H Q, Huang H. Enhanced Photocatalytic Performances of CeO_2/TiO_2 Nanobelt Heterostructures. *Small*, **2013**, **9**(22):3864-3872